HHS Public Access

Author manuscript

Cell Rep. Author manuscript; available in PMC 2016 September 29.

Published in final edited form as:

Cell Rep. 2015 September 29; 12(12): 2009–2020. doi:10.1016/j.celrep.2015.08.047.

Diminished MTORC1-Dependent JNK-Activation Underlies Neurodevelopmental Defects Associated with Lysosomal Dysfunction

Ching-On Wong[1], **Michela Palmieri**[2], **Jiaxing Li**[3], **Dmitry Akhmedov**[1], **Yufang Chao**[1], **Geoffrey T. Broadhead**[1], **Michael X. Zhu**[1,4], **Rebecca Berdeaux**[1,4], **Catherine A. Collins**[3], **Marco Sardiello**[2], and **Kartik Venkatachalam**[1,4,5,6]

[1]Department of Integrative Biology and Pharmacology, University of Texas School of Medicine, Houston, TX 77030

[2]Department of Molecular and Human Genetics, Baylor College of Medicine, Jan and Dan Duncan Neurological Research Institute, Texas Children's Hospital, Houston, Texas, TX 77030, USA

[3]Department of Molecular, Cellular and Developmental Biology, University of Michigan, Ann Arbor, MI 48109, USA

[4]Program in Cell and Regulatory Biology (CRB), Graduate School of Biomedical Sciences, University of Texas School of Medicine, Houston, TX 77030, USA

[5]Program in Neuroscience, Graduate School of Biomedical Sciences, University of Texas School of Medicine, Houston, TX 77030, USA

SUMMARY

We evaluate the mechanisms underlying neurodevelopmental deficits in *Drosophila* and mouse models of lysosomal storage diseases (LSDs). We find that lysosomes promote the growth of neuromuscular junctions (NMJs) via Rag GTPases and Mechanistic Target of Rapamycin Complex 1 (MTORC1). However, rather than employing S6K/4E-BP1, MTORC1 stimulates NMJ growth via JNK—a determinant of axonal growth in *Drosophila* and mammals. This role of lysosomal function in regulating JNK phosphorylation is conserved in mammals. Despite requiring the amino acid-responsive kinase, MTORC1, NMJ development is insensitive to dietary protein. We attribute this paradox to Anaplastic Lymphoma Kinase (ALK), which restricts neuronal amino acid uptake, and the administration of an ALK inhibitor couples NMJ development to dietary protein. Our findings provide an explanation for the neurodevelopmental deficits in LSDs and suggest an actionable target for treatment.

[6]To whom correspondence should be addressed: kartik.venkatachalam@uth.tmc.edu, Phone: 713-500-7504, Fax: 713-500-7456.

The authors declare no conflicts of interest.

INTRODUCTION

Mucolipidosis type IV (MLIV) and Batten disease are untreatable LSDs that cause childhood neurodegeneration (Vellodi, 2005; Venkatachalam et al., 2014). MLIV arises from loss-of-function mutations in the gene encoding TRPML1, an endolysosomal cation channel belonging to the TRP superfamily (Bargal et al., 2000; Bassi et al., 2000; Sun et al., 2000). The absence of TRPML1 leads to, defective lysosomal storage and autophagy, mitochondrial damage, and macromolecular aggregation, which together initiate the protracted neurodegeneration observed in MLIV (Curcio-Morelli et al., 2010; Jennings et al., 2006; Miedel et al., 2008; Vergarajauregui and Puertollano, 2008). Batten disease is another LSD, which arises from the absence of a lysosomal protein, CLN3 (Mitchison et al., 1997; Munroe et al., 1997), and results in psychomotor retardation (Kristensen and Lou, 1983). Both diseases cause early alterations in neuronal function. For instance, brain imaging studies revealed that MLIV and Batten patients display diminished axonal development in the cortex and corpus callosum (Autti et al., 1996; Frei et al., 1998), the causes of which remain unknown.

To develop better understand the etiology of MLIV in a genetically tractable model, we generated flies lacking the TRPML1 ortholog. *trpml*-deficient ($trpml^{1}$) flies have previously helped us gain insight into mechanisms underlying neurodegeneration and lysosomal storage (Venkatachalam et al., 2008; Venkatachalam et al., 2013; Wong et al., 2012). Here, we report that $trpml^{1}$ larvae exhibit diminished synaptic growth at the NMJ—a well-studied model synapse (Collins and DiAntonio, 2007). We now find that lysosomal function supports Rag GTPases and MTORC1 activation, and this is essential for JNK activation and synapse development. *Drosophila* larvae and mice lacking CLN3 also exhibit diminished Rag/MTORC1 and JNK activation suggesting that alterations in neuronal signaling are similar in different LSDs and are conserved. Interestingly, the NMJ defects in the two fly LSD models were suppressed by the administration of a high protein diet and a drug that is currently in clinical trials to treat certain forms of cancer. These findings inform a pharmacotherapeutic strategy that may suppress the neurodevelopmental defects observed in LSD patients.

RESULTS

Drosophila TRPML is a late-endosomal (LE)/lysosomal protein in neurons that is required for synapse development

In non-neuronal cells, TRPML shuttles between the plasma membrane and LE membranes (Wong et al., 2012). Here, we sought to evaluate the subcellular location of TRPML in neurons. The cell bodies of the *Drosophila* larval motor neurons (MNs) reside in the ventral nerve cord (VNC) and send axonal projections to the NMJs (Figure 1A). Coexpression of *UAS-trpml*::*myc* (TRPML::MYC) with the LE/lysosomal markers, *UAS-spinster*::*gfp* (Spin::GFP) or *UAS-lamp*::*gfp*, using $elav^{C155}$-*GAL4* (*elav-GAL4*), revealed that TRPML::MYC colocalized with the LE/lysosomal markers within neuronal cell bodies, axons, and NMJs (Figure 1A).

We found that *trpml* deficient larvae exhibited fewer NMJ boutons compared to wild-type (WT) (Figures 1B–1H). This phenotype was observed in the two loss-of-function alleles ($trpml^1$ and $trpml^2$), the $trpml^1/trpml^2$ transheterozygotes, and when the $trpml^1$ allele was in *trans* with a deficiency uncovering the *trpml* locus ($trpml^1/Df^{trpml}$) (Figure 1H). The $trpml^1$ NMJ growth phenotype was suppressed by a $trpml^+$ genomic rescue (P[$trpml^+$]; $trpml^1$) (Figures 1D and 1H). To identify the cells that require TRPML to promote NMJ growth, we selectively expressed *UAS-trpml* in $trpml^1$ neurons or muscle. We found that expression of *UAS-trpml* in mutant neurons using *elav-GAL4* or the MN specific, *C164-GAL4*, rescued the NMJ growth defect (Figures 1E–1F and 1H). However, expression of *UAS-trpml* in $trpml^1$ muscle using *mef2-GAL4* did not restore the bouton numbers (Figures 1G–1H). Thus, loss of TRPML results in a presynaptic defect in MNs leading to diminished NMJ growth.

Diminished synaptic growth in *trpml*^{1} is due to decreased activity of Rag GTPases/MTORC1

TRPML-dependent Ca^{2+} release allows the fusion of amphisomes with lysosomes, lysosomal degradation of proteins, and the production of free amino acids that activate Rag GTPases (Figure 2A) (Sancak et al., 2008; Wong et al., 2012). To address whether a decrease in Rag GTPase activation might underlie the diminished NMJ synaptic growth in $trpml^1$, we first examined NMJ growth in larvae lacking *ragC* (Kim et al., 2008). Compared to the heterozygous controls ($ragC^{\Delta}/+$), *ragC* deficient larvae ($ragC^{\Delta}$) showed fewer NMJ boutons (Figure 2B–2C and 2H). Similarly, neuronal expression of a dominant negative RagA ($RagA^{TN}$) decreased the bouton numbers (Figures 2D–2E and 2H). However, when expressed in $trpml^1$ neurons, $RagA^{TN}$ did not further decrease bouton numbers (Figure 2H). This lack of additivity suggests that Rag and TRPML function in a common pathway responsible for NMJ development. Indeed, expression of a constitutively active RagA ($RagA^{QL}$) in $trpml^1$ neurons completely rescued the synaptic growth defects (Figures 2F–2G and 2H). However, expression of $ragA^{QL}$ in WT neurons did not lead to an increase in bouton numbers (Figure 2H) indicating that the rescue the $trpml^1$ phenotype by $RagA^{QL}$ occurred by counteracting a decrease in Rag activity and not by some unrelated effects of $RagA^{QL}$ expression.

Rag GTPases are required for the function of MTORC1 (Sancak et al., 2008). Because Rag GTPases play a role in *Drosophila* NMJ development, we asked whether MTORC1 also plays a role in this process. We knocked down the critical MTORC1 subunit, Raptor (Hara et al., 2002), using an RNAi line ($raptor^{IR}$), which has been shown to lower *raptor* mRNA levels and MTORC1 activity (Natarajan et al., 2013). Consistent with the previously published effects of these RNAi lines on MTORC1 activity, we observed decreased pS6K in fat-body extracts from larvae expressing the $raptor^{IR}$ using *cg-GAL4* (Figure S1A). Moreover, expression of *UAS-*$raptor^{IR}$ in MNs using $vglut^{ok371}$*-GAL4* (*ok371-GAL4*) or in all neurons resulted in fewer boutons (Figure 2I). Therefore, activities of both Rag and MTORC1 are required for NMJ development.

The $trpml^1$ mutants exhibit late-pupal lethality (only 10–20% of $trpml^1$ pharate adults eclose), which can be partially suppressed by feeding the mutant larvae a protein-rich diet (allowing ~50% of $trpml^1$ pharate adults to eclose) (Wong et al., 2012). Expression of

RagA^{QL} in *trpml*^{1} neurons allowed ~80% of the pharate adults to eclose even without the administration of a high protein diet (Figure 2J). Therefore, the decrease in Rag activity in *trpml*^{1} neurons underlies both the synaptic growth defects and elevated pupal lethality. Moreover, rescue of both synaptic growth defects and pupal lethality by RagA^{QL} suggest a common molecular origin for the disparate *trpml*^{1} phenotypes.

Rag GTPases constitute the core of the Ragulator complex, which activates MTORC1 in response to an increase in amino acid levels (Bar-Peled et al., 2012) or a decrease in the activity of AMPK (Zhang et al., 2014) (Figure S1B). AMPK inhibits MTORC1 via phosphorylation and activation of the TSC1/TSC2 complex, which is a GAP for Rheb—a G-protein required for MTORC1 function (Zoncu et al., 2011). To evaluate a role for AMPK in the *trpml*^{1} NMJ phenotypes, we expressed either constitutively-active or dominant-negative AMPK (AMPK^{T184D} or AMPK^{K56R} respectively (Figure S1B)) in WT and *trpml*^{1} neurons. Although neuronal expression of AMPK^{T184D} results in diminished bouton numbers, expression of AMPK^{T184D} in *trpml*^{1} did not further decrease bouton numbers (Figure S1C). These data are consistent with the Ragulator complex being inhibited to a similar extent by the absence of TRPML or an increase in AMPK activity. However, expression of AMPK^{K56R} in *trpml*^{1} neurons did not restore bouton numbers (Figure S1C). Thus, compromised activities of Ragulator in *trpml*^{1} neurons are not due to AMPK overactivation, but likely reflect lower cellular amino acid levels dues to diminished lysosomal protein degradation.

MTORC1-dependent NMJ development is independent of S6K and 4E-BP1

MTORC1-dependent phosphorylation activates S6K and inhibits 4E-BP1 (Zoncu et al., 2011). However, previous studies have reported that neither S6K nor 4E-BP1 (Thor) determines NMJ bouton numbers (Cheng et al., 2011a; Lee et al., 2010). We also found that neuronal expression of neither dominant-negative S6K nor wild-type Thor (*elav>S6K*^{KQ} and *elav>thor* respectively) altered NMJ bouton numbers (Figure S1D).

The efficacy of rapamycin on MTORC1 activity depends on the phosphorylation target. Although effective at inhibiting phosphorylation of S6K and 4E-BP1, rapamycin does not effectively inhibit phosphorylation of some other MTORC1 targets (Kang et al., 2013). Because S6K and 4E-BP1 do not impact NMJ bouton numbers, we hypothesized that NMJ growth might be resistant to rapamycin. Indeed, synaptic overgrowth following overexpression of Rheb is not suppressed by rapamycin (Knox et al., 2007). We also found that feeding WT larvae 1 mM rapamycin, a concentration that effectively inhibits MTORC1 activity in larval fat bodies (Wong et al., 2012), did not alter NMJ bouton numbers (Figure S1E). Together, these findings indicate that MTORC1 regulates NMJ growth via a target(s) other than S6K and 4E-BP1 (Figure S1F).

TRPML, Rag, and MTORC1 promote NMJ synapse development via JNK

To identify the downstream target(s) of Rag/MTORC1 that impact(s) NMJ bouton numbers, we examined the pathways that influence NMJ synapse development in *Drosophila* larvae. The BMP/TGF-β retrograde cascade involves the phosphorylation of the transcription factor, MAD, which promotes NMJ growth (Marques et al., 2002; Sweeney and Davis, 2002).

However, the relative intensities of pMAD staining at the NMJ and the MN nuclei were unchanged in *trpml*^{1} (Figure S2A–S2D) indicating that the diminished synaptic growth in *trpml*^{1} is not due to decreased BMP/TGF-b signaling. Mutants lacking a *Drosophila* Wnt homolog, Wingless (Wg), or exhibiting destabilized presynaptic microtubules, have enlarged but fewer boutons (Miech et al., 2008; Packard et al., 2002; Pennetta et al., 2002; Roos et al., 2000; Wong et al., 2014). Although *trpml*^{1} displayed a decrease in bouton numbers, bouton morphology was not altered (Figures 1B–1G). Furthermore, the levels of presynaptic Wg remained unchanged in *trpml*^{1} (Figure S2E), suggesting that Wg release is not affected in *trpml*^{1}. Therefore, the *trpml*^{1} synaptic growth defects do not result from diminished Wg signaling or from alterations in presynaptic microtubule structure.

Next, we investigated whether presynaptic JNK signaling, which promotes NMJ development (Ballard et al., 2014; Sanyal et al., 2002), may be decreased in *trpml*^{1}. To do so, we first examined whether *trpml*^{1} exhibits dominant genetic interactions with loss-of-function mutations in JNK related genes. Although larvae carrying single copies of *trpml*^{1} or the loss-of-function allele of *Drosophila* JNK (*basket*^{1} (*bsk*^{1})) did not exhibit a decrease in bouton numbers, transheterozygous *bsk*^{1}/+; *trpml*^{1}/+ NMJs showed fewer boutons (Figures 3A–3C and 3G). We also observed a dominant genetic interaction between *bsk*^{1} and *ragC*$^{\Delta}$ (Figures 3D and 3G). The MAPKKK, Wallenda (Wnd), which is the *Drosophila* homolog of DLK1, is responsible for the activation of JNK in *Drosophila* MNs (Collins et al., 2006). Transheterozygous *wnd*^{3}/*trpml*^{1} NMJs also exhibited fewer synaptic boutons whereas neither heterozygous alone showed the phenotype (Figures 3E–3F and 3H).

The E3-ubiquitin ligase, Highwire (Hiw), restricts NMJ bouton numbers by promoting Wnd degradation (Collins et al., 2006). Neuronal expression of *UAS-hiw* in *trpml*^{1}/+ (*elav>hiw*; *trpml*^{1}/+) resulted in a decrease in bouton numbers that was not observed when *UAS-hiw* was expressed in WT neurons (*elav>hiw*) (Figure 3J). Therefore, *trpml*^{1}/+ neurons constitute a sensitized system, in which expression of a negative regulator of JNK signaling restricts the formation of synaptic boutons. Interestingly, expression of Hiw in the *trpml*^{1} homozygotes resulted in synthetic embryonic lethality (not shown)—likely due to massive downregulation of JNK signaling because *bsk*^{1} homozygotes also exhibit embryonic lethality (Riesgo-Escovar et al., 1996).

Because the *elav>hiw; trpml*^{1}/+ still contained one functional copy of *trpml*, we asked whether exogenously activating TRPML in these animals would restore the bouton numbers. Both mammalian TRPML1 and fly TRPML are PI(3,5)P_2 activated channels (Dong et al., 2010; Feng et al., 2014a), whose activity is further potentiated by ML-Synthetic Agonist 1 (ML-SA1) (Feng et al., 2014b; Shen et al., 2012) (Figure 3I). Feeding ML-SA1 (20 μM final concentration in fly food) to the *elav>hiw*; *trpml*^{1}/+ larvae restored synaptic growth, whereas the *trpml*^{1} homozygous larvae were insensitive to ML-SA1 (Figure 3J). Thus, TRPML channel activity supports JNK-dependent NMJ growth.

Synaptic overgrowth in *hiw*-deficient larvae is suppressed by lysosomal dysfunction or a decreased Rag/MTORC1 activity

Larvae lacking *hiw* (*hiw*^{ND8}) exhibit an elevated number of relatively smaller NMJ boutons (DiAntonio et al., 2001; Wan et al., 2000). Because decreasing JNK levels in *hiw*^{ND8}

suppresses the alterations in synaptic growth and morphology (Collins et al., 2006), we hypothesized that *trpml*^{1} might also suppress the *hiw*^{ND8}-induced synaptic phenotypes. Indeed, *hiw*^{ND8}*;;trpml*^{1} double mutants had significantly fewer boutons than *hiw*^{ND8} alone (Figures 4A–4B and 4E). The bouton numbers observed in *hiw*^{ND8} were also reduced following MN-specific expression of dominant negative *ragA*^{TN} or *raptor*^{IR} (Figures 4C–4E). Thus, lysosomal function and Rag/MTORC1 activity are partially required for the NMJ synapse expansion in *hiw*^{ND8}, further supporting the notion that lysosomal function and Rag/MTORC1 are required for maximal JNK activation. However, none of the manipulations described above rescued the "small-bouton" phenotype of *hiw*^{ND8}.

Synaptic overgrowth due to Rheb overexpression is suppressed by *wnd* mutants

Could the synaptic overgrowth associated with the neuronal overactivation of MTORC1 be suppressed by decreasing the levels of Wnd? As described previously (Knox et al., 2007; Natarajan et al., 2013), neuronal overexpression of Rheb (*elav>rheb*), which induces MTORC1 activation (Stocker et al., 2003) (Figure 4K), resulted in a 2-fold increase in the number of synaptic boutons (Figures 4F–4G and 4J). Interestingly, *wnd*^{3}/+ markedly suppressed the increase in bouton numbers in *elav>rheb* (Figures 4H–4J). Therefore, NMJ overgrowth following MTORC1 overactivation requires Wnd (Figure 4K).

Rag/MTORC1 activity promotes JNK phosphorylation and JNK-dependent gene transcription

Next, we asked whether manipulation of the Rag/MTORC1 pathway impacts JNK phosphorylation. Western blotting of larval brain extracts revealed that the levels of phospho-JNK (pJNK) were significantly decreased in the *ragC*$^{\Delta}$ (Figures 5A–5B). Consistent with increased Wnd levels in *hiw*^{ND8} mutants (Collins et al., 2006), pJNK levels were elevated in the *hiw*^{ND8} larval brain extracts (Figures 5A–5B). The pJNK elevation in *hiw*^{ND8} was significantly reduced following the introduction of *trpml*^{1} (Figures 5A–5B). However, the total JNK levels were not altered in these genotypes (Figures 5A and 5C). Conversely, the levels of pJNK/JNK were elevated in brain extracts derived from *elav>rheb* larvae (Figures 5A and 5D). Therefore, JNK phosphorylation correlates with MTORC1 activity.

The gene, *puckered* (*puc*), is expressed following JNK activation (Martin-Blanco et al., 1998), and the *puc-LacZ* reporter is used to assess JNK-dependent gene transcription (Ramet et al., 2002). Although we were unable to recombine the *puc-LacZ* transgene with *trpml*^{1}, we monitored nuclear β-Galactosidase (β-Gal) staining intensities in larvae carrying the *puc-LacZ* transgene, in which either dominant negative *ragA*^{TN} or *raptor*^{IR} were expressed under the control of the MN-specific, *BG380-GAL4*. We found that expression of *ragA*^{TN} or *raptor*^{IR} significantly decreased β-Gal intensities i.e. *puc-LacZ* induction (Figures 5E–5F). However, expression of an RNAi against *moody*, a gene unrelated to the MTORC1 pathway, did not alter the β-Gal intensity (β-Gal intensity relative to *BG380-GAL4/+* = 0.98, p = 0.8, unpaired Student's t-test). Expression of *UAS-rheb* under the control of *BG380-GAL4* led to a 2.5-fold increase in β-Gal intensity (Figures 5E and 5G). Therefore, JNK-dependent transcription correlates with MTORC1 activity.

MTORC1 phosphorylates Wnd

Evaluation of the primary amino acid sequence of Wnd revealed that although the protein contains a total of 69 serine and 8 threonine residues that can be phosphorylated (NetPhos2.0), only 4 of these sites bear the hallmarks of MTOR consensus sites (S305, T309, S362, S392) (Hsu et al., 2011). To test the hypothesis that MTORC1 phosphorylates Wnd at one or more of these residues, we first purified MTORC1 from cells stably expressing FLAG-tagged Raptor (FLAG-Raptor) (Yip et al., 2010). Both MTOR and FLAG-Raptor were present in the purified complex, along with the kinase ULK1/Atg1, which interacts with MTORC1 (Hosokawa et al., 2009) (Figure S3A). In contrast, JNK was absent in the purified complex, whereas it was detected in both the input and flow-through (Figure S3A). The MTORC1 complex we purified was functional as it phosphorylated recombinant 4E-BP1 *in vitro* (Figure S3B), and this phosphorylation was abolished by the MTOR kinase inhibitor, Torin1 (Thoreen et al., 2009) (Figure S3B).

Next, we purified a GST-tagged kinase-dead Wnd (GST-Wnd^{KD}—K188A, to rule out autophosphorylation of Wnd) from *E. coli* and evaluated its phosphorylation by MTORC1 *in vitro* (Stewart et al., 2013). We found that GST-Wnd^{KD} was phosphorylated only in the presence of MTORC1, and Torin1 significantly decreased this phosphorylation (Figures 5H–5I). However, GST alone was not phosphorylated by MTORC1 (Figure S3C). Interestingly, the phosphorylation of GST-Wnd^{KD} was only decreased by ~30% following Torin1 treatment, which indicates that the MTORC1 we purified also contains Torin1-insensitive kinase(s) that can phosphorylate GST-Wnd^{KD}. Consistent with this notion, although GST-Wnd^{KD} lacking the 4 putative MTOR phosphorylation sites (GST-mut-Wnd^{KD}; contains the following mutations: K188A, S305A, T309A, S362A, and S392A) was phosphorylated by MTORC1, this residual phosphorylation was insensitive to Torin1 (Figure 5H–5I). Therefore, Torin1-sensitive phosphorylation of GST-Wnd^{KD} by MTORC1 occurs at the four predicted MTOR target sites, whereas additional kinase(s) in the complex phosphorylate(s) Wnd on other phosphorylation sites in the protein. Our data indicate that MTORC1 directly phosphorylates Wnd, which stimulates JNK phosphorylation and promotes NMJ growth (Figure 5J).

Diminished NMJ bouton numbers, Rag/MTORC1 activation, and JNK activation are also observed in a *Drosophila* model of Batten disease

To examine whether decreased neuronal JNK signaling is a general outcome of lysosomal dysfunction, we first examined JNK phosphorylation in larvae that were fed chloroquine—a lysosomotropic agent that disrupts lysosomal degradation of proteins. Chloroquine-fed larvae exhibited a significant decrease in pJNK/JNK levels in the brain (Figure S4A–S4B). Thus, decreased lysosomal protein degradation results in diminished JNK phosphorylation.

Next, we sought to evaluate synaptic development and JNK signaling in flies lacking *cln3*. Similar to our findings in *trpml*^{1}, the number of NMJ boutons in *cln3* deficient larvae (*cln3*^{DMB1}) (Tuxworth et al., 2009) was significantly lower than those in heterozygous controls (*cln3*$^{\Delta MB1}$/+) (Figures 6A–6C). We also expressed an RNAi line against *Drosophila cln3* (*UAS-cln3*^{IR}) in MNs and observed a decrease in the number of synaptic boutons (Figure S3C–S3D and 6C). Therefore, loss of either *trpml* or *cln3* in MNs results in

diminished synaptic growth at the NMJ, indicating a general role of lysosomal function in synaptic development.

The *trpml*^{1} and *cln3*$^{\Delta MB1}$ mutants exhibited dominant genetic interactions whereas bouton numbers in the *cln3*$^{\Delta MB1}$/+ and *trpml*^{1}/+ heterozygotes alone remained unchanged (Figure 6D), and expression of RagA^{QL} in the *cln3*$^{\Delta MB1}$ resulted in complete restoration of bouton numbers (Figure 6D). Furthermore, neuronal expression of *UAS-cln3*^{IR} led to lower levels of pJNK (Figures 6E–6F), but not total JNK (data not shown), and a significant decreased bouton numbers in *hiw*^{ND8} (Figure S3E–S3G). Therefore, diminished synaptic bouton numbers in both *trpml*^{1} and *cln3*$^{\Delta MB1}$ occur via a similar pathway involving low Rag/MTORC1 activity and JNK phosphorylation.

Neuronal JNK phosphorylation is diminished in a mouse model of Batten disease

JNK activation is required for axonal tract development in the corpus callosum (CC) and cortex in mice (Eto et al., 2010). Brain sections from E19.5 embryos revealed lower pJNK levels in the CC in the *Cln3*-deficient animal (*Cln3*$^{\Delta 7–8/\Delta 7–8}$, hereafter referred to as *Cln3*$^{-/-}$) (Cotman et al., 2002) (Figures 6G–6J and 6K–6L). The decrease in pJNK levels in the *Cln3*$^{-/-}$ axons was particularly striking in the commissures adjacent to the CC (Figures 6H, 6J, and 6K-6L, compare regions indicated by *arrows* in the two genotypes). However, the total JNK levels were not changed in the *Cln3*$^{-/-}$ sections (Figure S3H–S3K). Cerebral cortex lysates from E17.5 *Cln3*$^{-/-}$ mice embryos also exhibited significantly reduced levels of pJNK and ratio of pJNK/JNK (Figures 6M–6O). Thus, decreased neuronal JNK activation following lysosomal dysfunction occurs in multiple LSD models, and is conserved between flies and mammals.

Simultaneous inhibition of ALK and administration of high-protein diet partially rescue the *trpml*^{1} synaptic growth defects and pupal lethality

Feeding *trpml*^{1} larvae a high-protein diet promotes the activation of Rag and suppresses the mutant phenotypes in non-neuronal cells (Wong et al., 2012). Because the NMJ growth defects in *trpml*^{1} also arise from a decrease in the activity of Rag, we examined whether feeding *trpml*^{1} larvae a high-protein diet could rescue the synaptic growth defects. To our surprise, we found that raising the *trpml*^{1} larvae on a high-protein diet did not affect the NMJ growth defects (Figure 7A). Therefore, although *trpml*^{1} neurons exhibit decreased activation of an amino acid responsive cascade, these cells are unable to adequately respond to an elevation in dietary protein content.

These data were consistent with previous findings that *Drosophila* neuroblasts are insensitive to dietary protein content compared to non-neuronal cells (Cheng et al., 2011b). This insensitivity is due to the evolutionarily conserved receptor-tyrosine kinase, ALK, which is enriched in neurons and represses neuronal amino acid uptake (Figure 7B, *left and middle panels*), while promoting neuroblast development by activating PI3K thereby allowing neuroblasts to withstand fluctuations in dietary amino acids (Cheng et al., 2011b) (Figure 7B, *middle panel*). Owing to the expression of ALK in mature neurons (Rohrbough et al., 2013), amino acid uptake might remain suppressed in these cells. If so, inhibition of

ALK in *trpml*^{1} could derepress the uptake of dietary amino acids resulting in the activation of Rag and recovery of synaptic growth (Figure 7B, *right panel*).

We tested this hypothesis by feeding larvae a highly selective ALK inhibitor, CH5424802 (Sakamoto et al., 2011). The amino acid residues on ALK that mediate the effect of CH5424802 are conserved in *Drosophila* ALK. Moreover, CH5424802 treatment resulted in decreased phosphorylation of Akt on S473 (Figure S4L–S4M)—a known consequence of inhibition of ALK, which is responsible for phosphorylation of Akt on S473 via PI3K (Slupianek et al., 2001). Next, we fed larvae CH5424802 (final concentration of 1 mM in fly food) either with or without a high-protein diet for ~48 hours. Remarkably, only the *trpml*^{1} larvae that were fed both CH5424802 and a high protein diet showed significant recovery of the synaptic bouton numbers (Figure 7C). However, the combination of high protein diet and CH5424802 did not elevate the bouton numbers when either dominant-negative *ragA*^{TN} was simultaneously expressed in the *trpml*^{1} neurons (Figure 7C) or in *ragC*^{D} (Figure 7D). We also observed significant rescue of bouton numbers in larvae expressing *cln3* RNAi in MNs following simultaneous administration of CH5424802 and high-protein diet (Figure 7E). Thus, inhibition of ALK is critical for restoration of Rag activity and synaptic growth by a high protein diet in neurons with lysosomal dysfunction.

Feeding the *trpml*^{1} larvae a combination of yeast and CH5424802 also significantly increased the percentage of flies surviving to adulthood compared to feeding the larvae a diet comprised of yeast without CH5424802 (Figure 7F). Therefore, a combination of high protein diet and ALK-inhibition rescues defects in both synapse development and adult viability in animals with lysosomal dysfunction.

DISCUSSION

Lysosomal dysfunction results in diminished synapse development

We show that lysosomal dysfunction in *Drosophila* MNs results in diminished bouton numbers at the larval NMJ. We present evidence that lysosomal dysfunction results in decreased activation of the amino acid responsive cascade involving Rag/MTORC1, which are critical for normal NMJ development (Figure 7G). Despite the requirement for MTORC1 in NMJ synapse development, previous studies and our current findings show that bouton numbers are independent of S6K and 4E-BP1. Rather, MTORC1 promotes NMJ growth via a MAP kinase cascade culminating in JNK activation (Figure 7G). Therefore, decreasing lysosomal function or Rag/MTORC1 activation in *hiw*^{ND8} suppressed the associated synaptic overgrowth. However, the “small-bouton” phenotype of *hiw*^{ND8} was independent of MTORC1. Thus, MTORC1 is required for JNK-dependent regulation of bouton numbers, whereas bouton morphology is independent of MTORC1. Furthermore, although both *rheb* expression and *hiw* loss result in Wnd-dependent elevation in bouton numbers, the supernumerary boutons in each case show distinct morphological features. Additional studies are needed for deciphering the complex interplay between MTORC1-JNK in regulating the NMJ morphology.

Biochemical analyses revealed that both JNK phosphorylation and its transcriptional output correlated with the activity of MTORC1, which are consistent with prior observations that

cln3 overexpression promotes JNK activation (Tuxworth et al., 2009) and that *tsc1/tsc2* deletion in flies result in increased JNK-dependent transcription (Gordon et al., 2013). These findings point to the remarkable versatility of MTORC1 in controlling both protein translation and gene transcription.

Using an *in vitro* kinase assay, we demonstrate that Wnd is a target of MTORC1. Because axonal injury activates both MTORC1 and DLK/JNK (Abe et al., 2010; Kenney and Kocsis, 1998; Valakh et al., 2015), our findings imply a functional connection between these two pathways. Interestingly, our data also suggest that MTORC1 contains additional kinases besides MTOR that can phosphorylate Wnd. One possibility is that ULK1/Atg1, which associates with MTORC1 (Figure S3A and (Hosokawa et al., 2009)), could be the kinase that phosphorylates Wnd. Consistent with this notion, overexpression of Atg1 in the *Drosophila* neurons has been shown to promote JNK signaling and NMJ synapse overgrowth via Wnd (Shen and Ganetzky, 2009).

We also found that developmental JNK activation in axonal tracts of the CC, as well as pJNK levels in cortical neurons were compromised in a mouse model of Batten disease. Thus, the signaling deficits we identified in *Drosophila* are also conserved in mammals. The activity of DLK (the mouse homolog of Wnd) and JNK signaling are critical for axonal development in the mouse CNS (Hirai et al., 2006). Therefore, decreased neuronal JNK activation during development might underlie the thinning of the axonal tracts observed in many LSDs.

Simultaneous administration of an ALK inhibitor and a high-protein diet rescues the synaptic growth defects and pupal lethality associated with lysosomal dysfunction

Although our findings demonstrate a role for an amino acid responsive cascade in the synaptic defects associated with lysosomal dysfunction, simply elevating the dietary protein content was not sufficient to rescue these defects. These findings were reminiscent of an elegant study that showed that the growth of *Drosophila* neuroblasts is uncoupled from dietary amino acids owing to the function of ALK, which suppresses the uptake of amino acids into the neuroblasts (Cheng et al., 2011b). Indeed, simultaneous administration of an ALK inhibitor and a high-protein diet partially rescued the synaptic growth defects associated with the lysosomal dysfunction, and improved the rescue of pupal lethality associated with $trpml^{1}$. Although our studies do not causally link the defects in synapse development with pupal lethality, they do raise the intriguing possibility that multiple phenotypes associated with LSDs could be targeted using ALK inhibitors along with a protein-rich diet.

Although LSDs result in lysosomal dysfunction throughout the body, neurons are exceptionally sensitive to these alterations (Bellettato and Scarpa, 2010). The cause for this sensitivity remains incompletely understood. Given our findings that mature neurons do not efficiently take up amino acids from the extracellular medium, lysosomal degradation of proteins serves as a major source of free amino acids in these cells. Therefore, disruption of lysosomal degradation leads to severe shortage of free amino acids in neurons, regardless of the quantity of dietary proteins, thus explaining the exquisite sensitivity of neurons to lysosomal dysfunction.

EXPERIMENTAL PROCEDURES

Immunohistochemistry and immunofluorescence

Drosophila—Wandering 3rd instar larvae were pinned on Sylgard (Dow Corning), and bathed in ice-cold PBS. The body wall was cut along the dorsal midline, and visceral organs were removed. The fillets were pinned flat and fixed with 4% paraformaldehyde in PBS for 30 mins. Fixed fillets were washed with 0.1% Triton X-100 in PBS before primary antibody incubation. Antibody dilutions: 1:200 rabbit α-HRP (Jackson), 1:100 mouse α-DLG, 1:500 rabbit α-GFP (Invitrogen), 1:500 mouse α-myc (Sigma), 1:1000 rabbit α-pMAD (Persson et al., 1998), 1:100 rabbit α-pMAD (S463/465) (41D10, Cell Signaling), 1:100 mouse α−β-Gal (40-1a), 1:500 mouse α-Wg. After incubation with primary antibodies overnight at 4°C, the fillets were washed and probed with appropriate fluorophore-conjugated secondary antibodies (Alexa Fluor 488/568/647 goat anti-mouse/rabbit/guinea pig) (Invitrogen) at room temperature for 1.5 hrs. Samples were mounted on glass slide with DAPI-containing Vectashield (Vector Labs). The monoclonal antibodies against DLG, β-Gal, and Wg were obtained from the Developmental Studies Hybridoma Bank (DSHB) developed under the auspices of the NICHD and maintained by The University of Iowa, Department of Biology, Iowa City, IA 52242.

Mice

Brains from E19.5 mice were fixed with 10% formalin (Sigma) at 4 °C overnight, and processed for decalcification for 2 days with Gooding and Stewart's fluid (15% formic acid, 5% formaldehyde 37%). They were then dehydrated gradually (70% to 100% ethanol), equilibrated with chloroform, embedded in paraffin blocks, and sectioned at 10 μm thickness. The sections were subjected to the immunohistochemistry using mouse monoclonal antibodies against JNK (BD, 1:200) and rabbit polyclonal antibodies against pJNK (Cell Signaling, 1:400). The Vectastain Elite ABC kit (Vector Lab) was used for the immunohistochemistry according to the manufacturer's protocol.

For immunofluorescence, the sections were permeabilized with 0.3% Triton X-100 in PBS and blocked for 2 hrs at room temperature with 1% serum, 0.05% Triton X-100 in PBS. The slides were washed in PBS and incubated with the primary antibody for 1 day at 4 °. After washing, secondary antibodies (donkey anti-rabbit Alexa Fluor 594), were added (1:200) for 2 hrs. The slides were then mounted in Vectashield.

Western blots

Drosophila—Brains or fat-bodies from wandering 3rd instar larvae were dissected in ice-cold HL-3 (70 mM NaCl, 5 mM KCl, 20 mM $MgCl_2$, 10 mM $NaHCO_3$, 0.1 mM $CaCl_2$, 115 mM sucrose, 5 mM trehalose, and 5 mM HEPES; pH 7.2.). 6–8 brains or 3–4 fat bodies per genotype were triturated in 30 μL Laemmli sample buffer (Bio-Rad) with 5% 2-mercaptoethanol (Calbiochem), and heated at 96°C for 10 mins. For a cute CH5424802 treatment, 4 brains were dissected in HL-3 (containing 1 mM $CaCl_2$) with or without 1 μM CH5424802 for 1 hr, before being triturated and heated in sample buffer. Total lysates were centrifuged at 10000g for 4 min before loading the supernatant onto 4–20% gradient gel (Bio-Rad) for SDS-PAGE. Separated proteins were transferred onto nitrocellulose blot

before blocking (Odyssey Blocking Buffer, LI-COR Biosciences). The blot was probed by primary antibody mixture containing 1:5000 rabbit α-pJNK (Promega), 1:200 rabbit α-JNK (Santa Cruz), 1:1000 rabbit α-phospho-*Drosophila* p70 S6K (Cell Signaling), 1:1000 rabbit α-pAKT^{S473} (Cell Signaling), or 1:1000 mouse α-alpha-tubulin (12G10, DSHB). The secondary antibodies used were IRDye 680LT (anti-rabbit) and IRDye 800CW (anti-mouse) (LI-COR Biosciences). The bands were detected by the Odyssey imaging platform (LI-COR Biosciences). Band intensities were quantified using ImageJ.

Mice

Cerebral cortices were dissected from E17.5 mouse embryos, and homogenized in icecold lysis buffer (20 mM Tris-HCl, pH 7.4, 150 mM NaCl, 2 mM EDTA, 1% Triton X-100, 10% glycerol in presence of protease and phosphatase inhibitor (Roche)). Following SDS-PAGE, membranes were blocked in 5% BSA and incubated with primary antibodies: mouse monoclonal JNK (BD Biosciences, 1:500) and rabbit polyclonal pJNK (Cell Signaling, 1:1000) overnight at 4°C. Blot ima ges were acquired using the LAS 4000 gel imaging system (GE Healthcare) and quantified using ImageJ.

In vitro kinase assay

MTORC1 was preincubated (30°C, 15 min) with Torin1 (10 μM) or vehicle in kinase assay buffer (in mM: 50 KCl, 10 $MgCl_2$, 1 DTT, 25 HEPES, pH7.4). For the radioactive kinase assay, the purified proteins (GST-Wnd^{KD}, GST-mut-Wnd^{KD}, or GST) and the kinase assay buffer containing 50 μM ATP and [γ-^{32}P] ATP (10 μCi per reaction) were added to the preincubated MTORC1 reaction mixture. Kinase reaction was performed (30°C, 30 min) and stopped by boiling in Laemmli sample buffer and resolved on SDS-PAGE gels followed by silver staining. Phosphorylated proteins were visualized by autoradiography of dried gels and ^{32}P signals were quantified by densitometry. For the *in vitro* kinase assay on recombinant 4E-BP1, kinase assay buffer containing 150 ng of recombinant 4E-BP1 (Santa Cruz) and 500 μM ATP was mixed with MTORC1 preincubated with Torin1 (10 μM) or vehicle. Reactions were performed at 29°C for 30 minutes, and stopped by boiling the samples in Laemmli buffer. Samples were subsequently analyzed by SDS-PAGE and Western blotting with anti-phospho-4E-BP1 (T37/46) and anti-4E-BP1 antibodies (Cell Signaling).

Statistical Analysis

Paired or unpaired Student's t-tests were employed for pairwise comparisons. For comparison of 3 or more values, one-way ANOVA was performed to determine significance. The Bonferroni post-hoc correction was applied when performing multiple pairwise comparisons. All values shown in bar graphs represent mean ±SEM. Please consult the Supporting Information for all values in the bar graphs and information on statistical tests employed.

Supplementary Material

Refer to Web version on PubMed Central for supplementary material.

ACKNOWLEDGEMENTS

We thank the Bloomington *Drosophila* Stock Center and Drs. H. Bellen, Y. Wairkar, G. Tear, and A. Diantonio for fly stocks, and Dr. D. Sabatini for cells stably expressing FLAG- Raptor. We are grateful to N. Haelterman, K. Chen, L. Mangieri, and Drs. M. Jaiswal, S. Yamamoto, and N. Giagtzoglou for scientific discussions, and Dr. CK. Yao and H. Hu for technical help. This study was supported by the NIH grants, R01NS081301 (K.V.), R01NS079618 (M.S.), R01NS069844 (C.A.C.), and R01DK092590 and R01AR059847 (both to R.B).

REFERENCES

Abe N, Borson SH, Gambello MJ, Wang F, Cavalli V. Mammalian target of rapamycin (mTOR) activation increases axonal growth capacity of injured peripheral nerves. J Biol Chem. 2010; 285:28034–28043. [PubMed: 20615870]

Autti T, Raininko R, Vanhanen SL, Santavuori P. MRI of neuronal ceroid lipofuscinosis. I. Cranial MRI of 30 patients with juvenile neuronal ceroid lipofuscinosis. Neuroradiology. 1996; 38:476–482. [PubMed: 8837098]

Ballard SL, Miller DL, Ganetzky B. Retrograde neurotrophin signaling through Tollo regulates synaptic growth in Drosophila. J Cell Biol. 2014; 204:1157–1172. [PubMed: 24662564]

Bar-Peled L, Schweitzer LD, Zoncu R, Sabatini DM. Ragulator is a GEF for the rag GTPases that signal amino acid levels to mTORC1. Cell. 2012; 150:1196–1208. [PubMed: 22980980]

Bargal R, Avidan N, Ben-Asher E, Olender Z, Zeigler M, Frumkin A, Raas-Rothschild A, Glusman G, Lancet D, Bach G. Identification of the gene causing mucolipidosis type IV. Nat Genet. 2000; 26:118–123. [PubMed: 10973263]

Bassi MT, Manzoni M, Monti E, Pizzo MT, Ballabio A, Borsani G. Cloning of the gene encoding a novel integral membrane protein, mucolipidin-and identification of the two major founder mutations causing mucolipidosis type IV. Am J Hum Genet. 2000; 67:1110–1120. [PubMed: 11013137]

Bellettato CM, Scarpa M. Pathophysiology of neuropathic lysosomal storage disorders. J Inherit Metab Dis. 2010; 33:347–362. [PubMed: 20429032]

Cheng L, Locke C, Davis GW. S6 kinase localizes to the presynaptic active zone and functions with PDK1 to control synapse development. J Cell Biol. 2011a; 194:921–935. [PubMed: 21930778]

Cheng LY, Bailey AP, Leevers SJ, Ragan TJ, Driscoll PC, Gould AP. Anaplastic lymphoma kinase spares organ growth during nutrient restriction in Drosophila. Cell. 2011b; 146:435–447. [PubMed: 21816278]

Collins CA, DiAntonio A. Synaptic development: insights from Drosophila. Curr Opin Neurobiol. 2007; 17:35–42. [PubMed: 17229568]

Collins CA, Wairkar YP, Johnson SL, DiAntonio A. Highwire restrains synaptic growth by attenuating a MAP kinase signal. Neuron. 2006; 51:57–69. [PubMed: 16815332]

Cotman SL, Vrbanac V, Lebel LA, Lee RL, Johnson KA, Donahue LR, Teed AM, Antonellis K, Bronson RT, Lerner TJ, et al. Cln3(Deltaex7/8) knock-in mice with the common JNCL mutation exhibit progressive neurologic disease that begins before birth. Hum Mol Genet. 2002; 11:2709–2721. [PubMed: 12374761]

Curcio-Morelli C, Charles FA, Micsenyi MC, Cao Y, Venugopal B, Browning MF, Dobrenis K, Cotman SL, Walkley SU, Slaugenhaupt SA. Macroautophagy is defective in mucolipin-1-deficient mouse neurons. Neurobiol Dis. 2010; 40:370–377. [PubMed: 20600908]

DiAntonio A, Haghighi AP, Portman SL, Lee JD, Amaranto AM, Goodman CS. Ubiquitination-dependent mechanisms regulate synaptic growth and function. Nature. 2001; 412:449–452. [PubMed: 11473321]

Dong XP, Shen D, Wang X, Dawson T, Li X, Zhang Q, Cheng X, Zhang Y, Weisman LS, Delling M, et al. PI(3,5)P(2) controls membrane trafficking by direct activation of mucolipin Ca(2+) release channels in the endolysosome. Nat Commun. 2010; 1:38. [PubMed: 20802798]

Eto K, Kawauchi T, Osawa M, Tabata H, Nakajima K. Role of dual leucine zipper-bearing kinase (DLK/MUK/ZPK) in axonal growth. Neurosci Res. 2010; 66:37–45. [PubMed: 19808064]

Feng X, Huang Y, Lu Y, Xiong J, Wong CO, Yang P, Xia J, Chen D, Du G, Venkatachalam K, et al. Drosophila TRPML Forms PI(3,5)P2-activated Cation Channels in Both Endolysosomes and Plasma Membrane. J Biol Chem. 2014a; 289:4262–4272. [PubMed: 24375408]

Feng X, Xiong J, Lu Y, Xia X, Zhu MX. Differential mechanisms of action of the mucolipin synthetic agonist, ML-SA1, on insect TRPML and mammalian TRPML1. Cell Calcium. 2014b; 56:446–456. [PubMed: 25266962]

Frei KP, Patronas NJ, Crutchfield KE, Altarescu G, Schiffmann R. Mucolipidosis type IV: characteristic MRI findings. Neurology. 1998; 51:565–569. [PubMed: 9710036]

Geuking P, Narasimamurthy R, Lemaitre B, Basler K, Leulier F. A non-redundant role for Drosophila Mkk4 and hemipterous/Mkk7 in TAK1-mediated activation of JNK. PLoS One. 2009; 4:e7709. [PubMed: 19888449]

Gordon GM, Zhang T, Zhao J, Du W. Deregulated G1-S control and energy stress contribute to the synthetic-lethal interactions between inactivation of RB and TSC1 or TSC2. J Cell Sci. 2013; 126:2004–2013. [PubMed: 23447678]

Hara K, Maruki Y, Long X, Yoshino K, Oshiro N, Hidayat S, Tokunaga C, Avruch J, Yonezawa K. Raptor, a binding partner of target of rapamycin (TOR), mediates TOR action. Cell. 2002; 110:177–189. [PubMed: 12150926]

Hirai S, Cui de F, Miyata T, Ogawa M, Kiyonari H, Suda Y, Aizawa S, Banba Y, Ohno S. The c-Jun N-terminal kinase activator dual leucine zipper kinase regulates axon growth and neuronal migration in the developing cerebral cortex. J Neurosci. 2006; 26:11992–12002. [PubMed: 17108173]

Hosokawa N, Hara T, Kaizuka T, Kishi C, Takamura A, Miura Y, Iemura S, Natsume T, Takehana K, Yamada N, et al. Nutrient-dependent mTORC1 association with the ULK1-Atg13-FIP200 complex required for autophagy. Mol Biol Cell. 2009; 20:1981–1991. [PubMed: 19211835]

Hsu PP, Kang SA, Rameseder J, Zhang Y, Ottina KA, Lim D, Peterson TR, Choi Y, Gray NS, Yaffe MB, et al. The mTOR-regulated phosphoproteome reveals a mechanism of mTORC1-mediated inhibition of growth factor signaling. Science. 2011; 332:1317–1322. [PubMed: 21659604]

Jennings JJ Jr, Zhu JH, Rbaibi Y, Luo X, Chu CT, Kiselyov K. Mitochondrial aberrations in mucolipidosis Type IV. J Biol Chem. 2006; 281:39041–39050. [PubMed: 17056595]

Kang SA, Pacold ME, Cervantes CL, Lim D, Lou HJ, Ottina K, Gray NS, Turk BE, Yaffe MB, Sabatini DM. mTORC1 phosphorylation sites encode their sensitivity to starvation and rapamycin. Science. 2013; 341:1236566. [PubMed: 23888043]

Kenney AM, Kocsis JD. Peripheral axotomy induces long-term c-Jun amino-terminal kinase-1 activation and activator protein-1 binding activity by c-Jun and junD in adult rat dorsal root ganglia In vivo. J Neurosci. 1998; 18:1318–1328. [PubMed: 9454841]

Kim E, Goraksha-Hicks P, Li L, Neufeld TP, Guan KL. Regulation of TORC1 by Rag GTPases in nutrient response. Nat Cell Biol. 2008; 10:935–945. [PubMed: 18604198]

Knox S, Ge H, Dimitroff BD, Ren Y, Howe KA, Arsham AM, Easterday MC, Neufeld TP, O'Connor MB, Selleck SB. Mechanisms of TSC-mediated control of synapse assembly and axon guidance. PLoS One. 2007; 2:e375. [PubMed: 17440611]

Kristensen K, Lou HC. Central nervous system dysfunction as early sign of neuronal ceroid lipofuscinosis (Batten's disease). Dev Med Child Neurol. 1983; 25:588–590. [PubMed: 6354796]

Lee S, Liu HP, Lin WY, Guo H, Lu B. LRRK2 kinase regulates synaptic morphology through distinct substrates at the presynaptic and postsynaptic compartments of the Drosophila neuromuscular junction. J Neurosci. 2010; 30:16959–16969. [PubMed: 21159966]

Marques G, Bao H, Haerry TE, Shimell MJ, Duchek P, Zhang B, O'Connor MB. The Drosophila BMP type II receptor Wishful Thinking regulates neuromuscular synapse morphology and function. Neuron. 2002; 33:529–543. [PubMed: 11856528]

Martin-Blanco E, Gampel A, Ring J, Virdee K, Kirov N, Tolkovsky AM, Martinez-Arias A. puckered encodes a phosphatase that mediates a feedback loop regulating JNK activity during dorsal closure in Drosophila. Genes Dev. 1998; 12:557–570. [PubMed: 9472024]

Miech C, Pauer HU, He X, Schwarz TL. Presynaptic local signaling by a canonical wingless pathway regulates development of the Drosophila neuromuscular junction. J Neurosci. 2008; 28:10875–10884. [PubMed: 18945895]

Miedel MT, Rbaibi Y, Guerriero CJ, Colletti G, Weixel KM, Weisz OA, Kiselyov K. Membrane traffic and turnover in TRP-ML1-deficient cells: a revised model for mucolipidosis type IV pathogenesis. J Exp Med. 2008; 205:1477–1490. [PubMed: 18504305]

Mitchison HM, Taschner PE, Kremmidiotis G, Callen DF, Doggett NA, Lerner TJ, Janes RB, Wallace BA, Munroe PB, O'Rawe AM, et al. Structure of the CLN3 gene and predicted structure, location and function of CLN3 protein. Neuropediatrics. 1997; 28:12–14. [PubMed: 9151311]

Munroe PB, Mitchison HM, O'Rawe AM, Anderson JW, Boustany RM, Lerner TJ, Taschner PE, de Vos N, Breuning MH, Gardiner RM, et al. Spectrum of mutations in the Batten disease gene, CLN3. Am J Hum Genet. 1997; 61:310–316. [PubMed: 9311735]

Natarajan R, Trivedi-Vyas D, Wairkar YP. Tuberous sclerosis complex regulates Drosophila neuromuscular junction growth via the TORC2/Akt pathway. Hum Mol Genet. 2013; 22:2010–2023. [PubMed: 23393158]

Packard M, Koo ES, Gorczyca M, Sharpe J, Cumberledge S, Budnik V. The Drosophila Wnt, wingless, provides an essential signal for pre- and postsynaptic differentiation. Cell. 2002; 111:319–330. [PubMed: 12419243]

Pennetta G, Hiesinger PR, Fabian-Fine R, Meinertzhagen IA, Bellen HJ. Drosophila VAP-33A directs bouton formation at neuromuscular junctions in a dosage-dependent manner. Neuron. 2002; 35:291–306. [PubMed: 12160747]

Persson U, Izumi H, Souchelnytskyi S, Itoh S, Grimsby S, Engstrom U, Heldin CH, Funa K, ten Dijke P. The L45 loop in type I receptors for TGF-beta family members is a critical determinant in specifying Smad isoform activation. FEBS Lett. 1998; 434:83–87. [PubMed: 9738456]

Ramet M, Lanot R, Zachary D, Manfruelli P. JNK signaling pathway is required for efficient wound healing in Drosophila. Dev Biol. 2002; 241:145–156. [PubMed: 11784101]

Riesgo-Escovar JR, Jenni M, Fritz A, Hafen E. The Drosophila Jun-N-terminal kinase is required for cell morphogenesis but not for DJun-dependent cell fate specification in the eye. Genes Dev. 1996; 10:2759–2768. [PubMed: 8946916]

Rohrbough J, Kent KS, Broadie K, Weiss JB. Jelly Belly trans-synaptic signaling to anaplastic lymphoma kinase regulates neurotransmission strength and synapse architecture. Dev Neurobiol. 2013; 73:189–208. [PubMed: 22949158]

Roos J, Hummel T, Ng N, Klambt C, Davis GW. Drosophila Futsch regulates synaptic microtubule organization and is necessary for synaptic growth. Neuron. 2000; 26:371–382. [PubMed: 10839356]

Sakamoto H, Tsukaguchi T, Hiroshima S, Kodama T, Kobayashi T, Fukami TA, Oikawa N, Tsukuda T, Ishii N, Aoki Y. CH5424802, a selective ALK inhibitor capable of blocking the resistant gatekeeper mutant. Cancer Cell. 2011; 19:679–690. [PubMed: 21575866]

Sancak Y, Peterson TR, Shaul YD, Lindquist RA, Thoreen CC, Bar-Peled L, Sabatini DM. The Rag GTPases bind raptor and mediate amino acid signaling to mTORC1. Science. 2008; 320:1496–1501. [PubMed: 18497260]

Sanyal S, Sandstrom DJ, Hoeffer CA, Ramaswami M. AP-1 functions upstream of CREB to control synaptic plasticity in Drosophila. Nature. 2002; 416:870–874. [PubMed: 11976688]

Shen D, Wang X, Li X, Zhang X, Yao Z, Dibble S, Dong XP, Yu T, Lieberman AP, Showalter HD, et al. Lipid storage disorders block lysosomal trafficking by inhibiting a TRP channel and lysosomal calcium release. Nat Commun. 2012; 3:731. [PubMed: 22415822]

Shen W, Ganetzky B. Autophagy promotes synapse development in Drosophila. J Cell Biol. 2009; 187:71–79. [PubMed: 19786572]

Slupianek A, Nieborowska-Skorska M, Hoser G, Morrione A, Majewski M, Xue L, Morris SW, Wasik MA, Skorski T. Role of phosphatidylinositol 3-kinase-Akt pathway in nucleophosmin/anaplastic lymphoma kinase-mediated lymphomagenesis. Cancer Res. 2001; 61:2194–2199. [PubMed: 11280786]

Stewart R, Akhmedov D, Robb C, Leiter C, Berdeaux R. Regulation of SIK1 abundance and stability is critical for myogenesis. Proc Natl Acad Sci U S A. 2013; 110:117–122. [PubMed: 23256157]

Stocker H, Radimerski T, Schindelholz B, Wittwer F, Belawat P, Daram P, Breuer S, Thomas G, Hafen E. Rheb is an essential regulator of S6K in controlling cell growth in Drosophila. Nat Cell Biol. 2003; 5:559–565. [PubMed: 12766775]

Sun M, Goldin E, Stahl S, Falardeau JL, Kennedy JC, Acierno JS Jr, Bove C, Kaneski CR, Nagle J, Bromley MC, et al. Mucolipidosis type IV is caused by mutations in a gene encoding a novel transient receptor potential channel. Hum Mol Genet. 2000; 9:2471–2478. [PubMed: 11030752]

Sweeney ST, Davis GW. Unrestricted synaptic growth in *spinster*-a late endosomal protein implicated in TGF-β-mediated synaptic growth regulation. Neuron. 2002; 36:403–416. [PubMed: 12408844]

Thoreen CC, Kang SA, Chang JW, Liu Q, Zhang J, Gao Y, Reichling LJ, Sim T, Sabatini DM, Gray NS. An ATP-competitive mammalian target of rapamycin inhibitor reveals rapamycin-resistant functions of mTORC1. J Biol Chem. 2009; 284:8023–8032. [PubMed: 19150980]

Tuxworth RI, Vivancos V, O'Hare MB, Tear G. Interactions between the juvenile Batten disease gene, CLN3, and the Notch and JNK signalling pathways. Hum Mol Genet. 2009; 18:667–678. [PubMed: 19028667]

Valakh V, Frey E, Babetto E, Walker LJ, DiAntonio A. Cytoskeletal disruption activates the DLK/JNK pathway, which promotes axonal regeneration and mimics a preconditioning injury. Neurobiol Dis. 2015; 77:13–25. [PubMed: 25726747]

Vellodi A. Lysosomal storage disorders. Br J Haematol. 2005; 128:413–431. [PubMed: 15686451]

Venkatachalam K, Long AA, Elsaesser R, Nikolaeva D, Broadie K, Montell C. Motor deficit in a *Drosophila* model of mucolipidosis type IV due to defective clearance of apoptotic cells. Cell. 2008; 135:838–851. [PubMed: 19041749]

Venkatachalam K, Wong CO, Montell C. Feast or famine: role of TRPML in preventing cellular amino acid starvation. Autophagy. 2013; 9:98–100. [PubMed: 23047439]

Venkatachalam K, Wong CO, Zhu MX. The role of TRPMLs in endolysosomal trafficking and function. Cell Calcium. 2014

Vergarajauregui S, Puertollano R. Mucolipidosis type IV: the importance of functional lysosomes for efficient autophagy. Autophagy. 2008; 4:832–834. [PubMed: 18635948]

Wan HI, DiAntonio A, Fetter RD, Bergstrom K, Strauss R, Goodman CS. Highwire regulates synaptic growth in Drosophila. Neuron. 2000; 26:313–329. [PubMed: 10839352]

Wong CO, Chen K, Lin YQ, Chao Y, Duraine L, Lu Z, Yoon WH, Sullivan JM, Broadhead GT, Sumner CJ, et al. A TRPV channel in Drosophila motor neurons regulates presynaptic resting Ca2+ levels, synapse growth, and synaptic transmission. Neuron. 2014; 84:764–777. [PubMed: 25451193]

Wong CO, Li R, Montell C, Venkatachalam K. Drosophila TRPML Is Required for TORC1 Activation. Curr Biol. 2012; 22:1616–1621. [PubMed: 22863314]

Yip CK, Murata K, Walz T, Sabatini DM, Kang SA. Structure of the human mTOR complex I and its implications for rapamycin inhibition. Mol Cell. 2010; 38:768–774. [PubMed: 20542007]

Zhang CS, Jiang B, Li M, Zhu M, Peng Y, Zhang YL, Wu YQ, Li TY, Liang Y, Lu Z, et al. The lysosomal v-ATPase-Ragulator complex is a common activator for AMPK and mTORC1, acting as a switch between catabolism and anabolism. Cell Metab. 2014; 20:526–540. [PubMed: 25002183]

Zoncu R, Efeyan A, Sabatini DM. mTOR: from growth signal integration to cancer, diabetes and ageing. Nat Rev Mol Cell Biol. 2011; 12:21–35. [PubMed: 21157483]

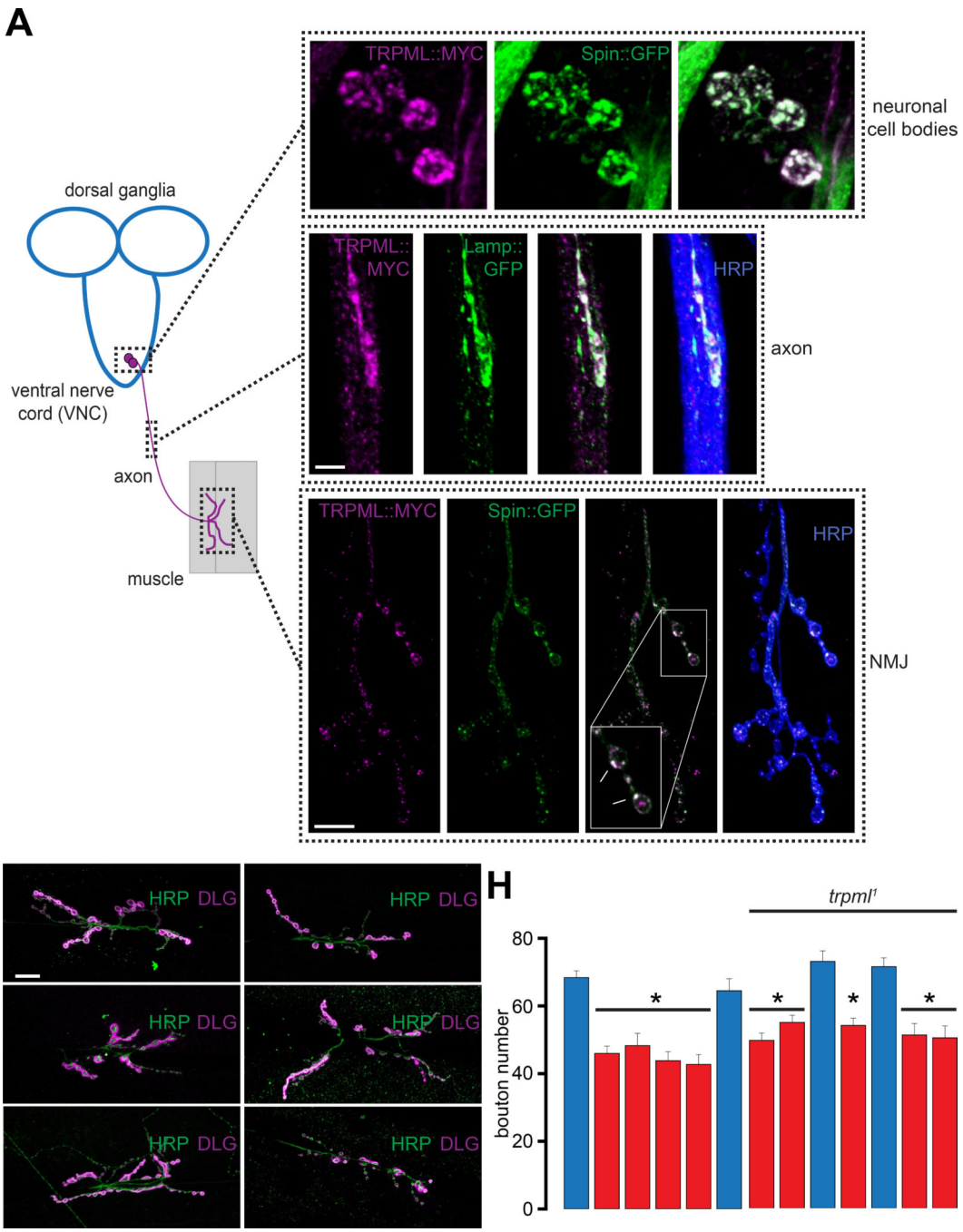

Figure 1. TRPML is required for larval NMJ development in *Drosophila*

(A) TRPML: :MYC colocalizes with LE/lysosomal markers in neuronal cell bodies, axons, and NMJs. Image on the left shows *Drosophila* larval MNs, whose cell bodies reside in the VNC and project axons to peripheral muscles. Only one set of MNs, muscle, and NMJ is shown for simplicity. Images on the top right are confocal images of neuronal cell bodies in the larval VNC dissected from animals expressing TRPML: :MYC (magenta) and Spin: :GFP (green) in neurons. Scale bar shown in left panel applies to all panels. Images in the middle are confocal images of larval axons in animals expressing TRPML: :MYC

(magenta) and Lamp: :GFP (green) in neurons. Scale bar shown in the left panel applies to all panels. Images on the bottom right are confocal images of larval NMJs from animals expressing TRPML: :MYC (magenta) and Spin: :GFP (green) in neurons. α-Horseradish peroxidase (HRP, blue) primary antibodies were used to stain axonal membranes. Scale bar shown in the left panel applies to all panels.

(B–G) Confocal images of larval NMJs from animals of the indicated genotypes stained with primary antibodies against HRP (green) and DLG (magenta). Scale bar shown in (B) also applies to (C–G).

(H) Bar graph showing the average bouton numbers in larval NMJs from animals of the indicated genotypes.

"*" represents statistical significance.

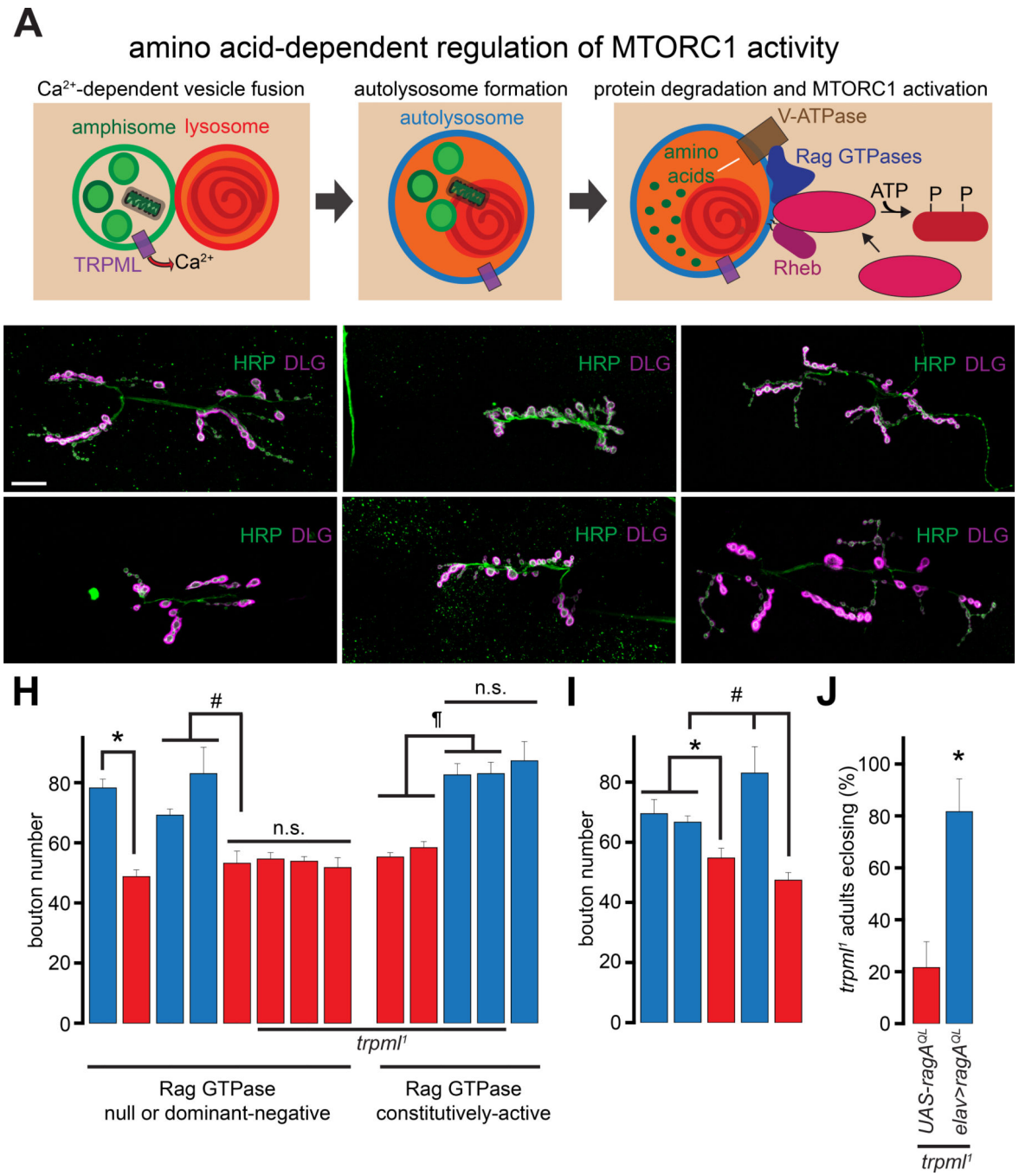

Figure 2. Diminished NMJ synaptic growth following lysosomal dysfunction is due to decreased activation of Rag/MTORC1

(A) TRPML is required for vesicle fusion, and in the presence of lysosomal free amino acids, MTORC1 is activated resulting in the phosphorylation of downstream targets.

(B–G) Confocal images of larval NMJs from animals of the indicated genotypes stained with antibodies against HRP (green) and DLG (magenta). Scale bar shown in (B) also applies to (C–G).

(H–I) Bar graphs showing the average bouton numbers in animals of the indicated genotypes.

(J) Bar graph showing the percentage of the *trpml*^{1} adults carrying the indicated transgenes that eclose from the pupal cases.

"*", "#", and "¶" represent statistical significance. Abbreviations: n.s., not significant.

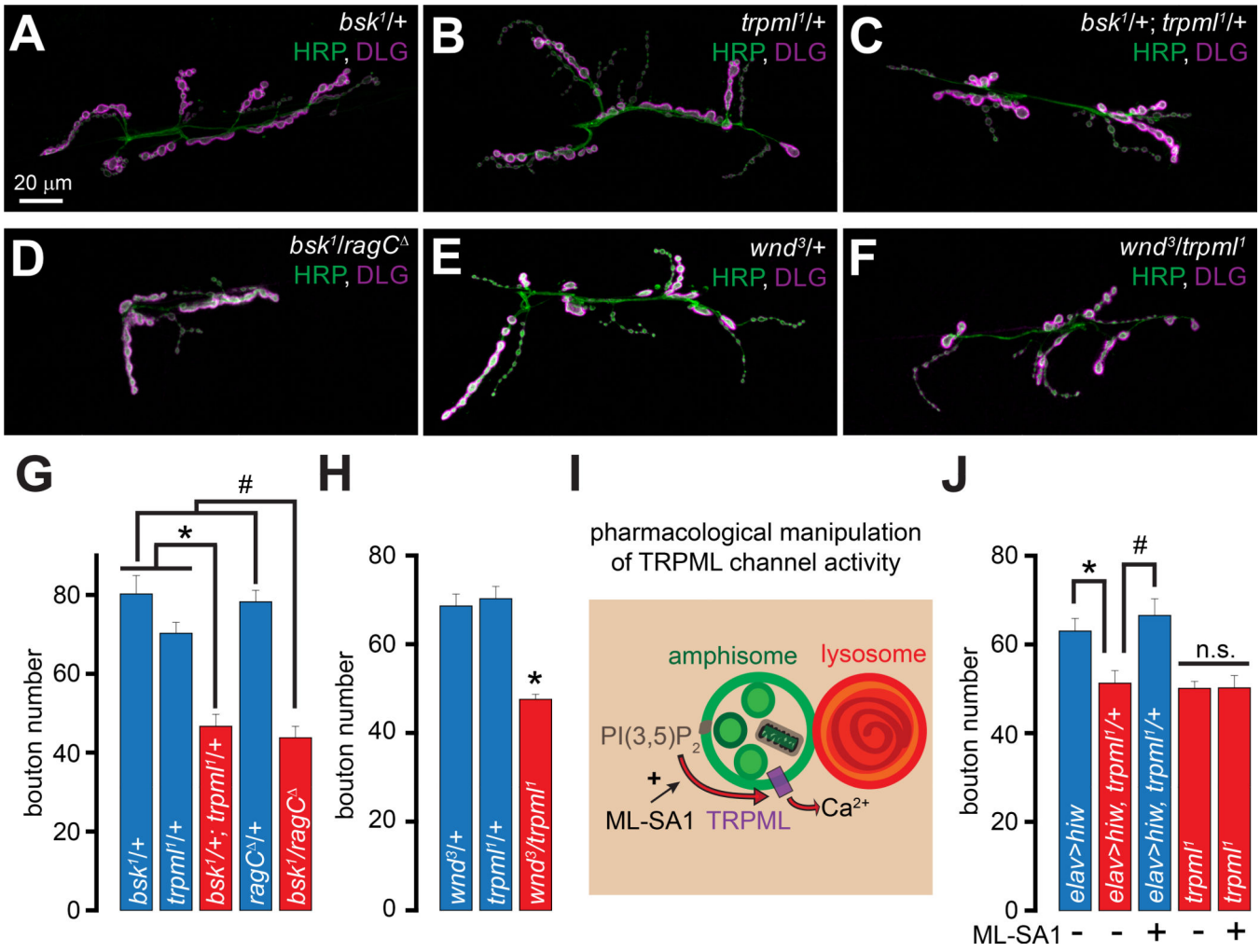

Figure 3. *trpml* and *ragC* exhibit dominant genetic interactions with genes encoding proteins involved in MAP kinase signaling

(A–F) Confocal images of larval NMJs from animals of the indicated genotypes stained with antibodies against HRP (green) and DLG (magenta). Scale bar shown in (A) also applies to (B–F).

(G–H) Bar graphs showing the average bouton numbers in animals of the indicated genotypes.

(I) $PI(3,5)P_2$ activates TRPML leading to vesicular Ca^{2+} release and ML-SA1 potentiates this effect.

(J) Bar graph showing the average bouton numbers in animals of the indicated genotypes reared on instant food with or without ML-SA1 feeding as indicated. Rearing larvae on instant food resulted in an overall increase in the number of boutons in all the genotypes (Wong et al., 2014). However, the *trpml*^{1} mutants still showed a relative decrease in NMJ boutons, and all comparisons were made between animals reared under identical conditions. "*" and "#" represent statistical significance. Abbreviations: n.s., not significant.

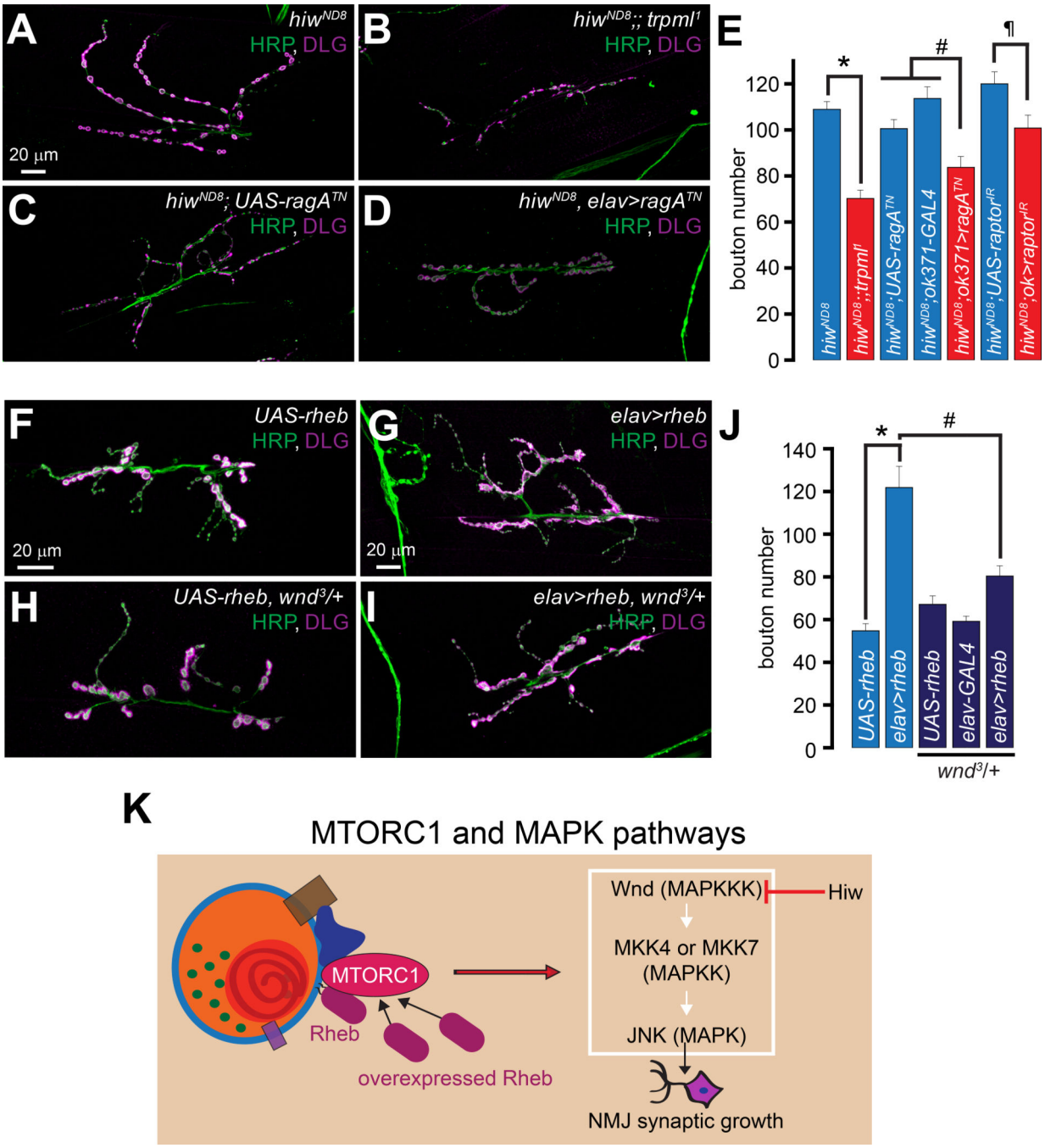

Figure 4. Lysosomal function and Rag/MTORC1 promote NMJ synapse growth via Wnd/JNK signaling

(A–D) Confocal images of larval NMJs from animals of the indicated genotypes stained with antibodies against HRP (green) and DLG (magenta). Scale bar shown in (A) also applies to (B–D).

(E) Bar graph showing the average bouton numbers in animals of the indicated genotypes.

(F–I) Confocal images of larval NMJs from animals of the indicated genotypes stained with antibodies against HRP (green) and DLG (magenta). Scale bar shown in (F) also applies to (H) and scale bar shown in (G) also applies to (I).

(J) Bar graph showing the average bouton numbers in animals of the indicated genotypes.
(K) Crosstalk between the MTORC1 and Wnd/JNK pathways.
"*", "#", and "¶" represent statistical significance.

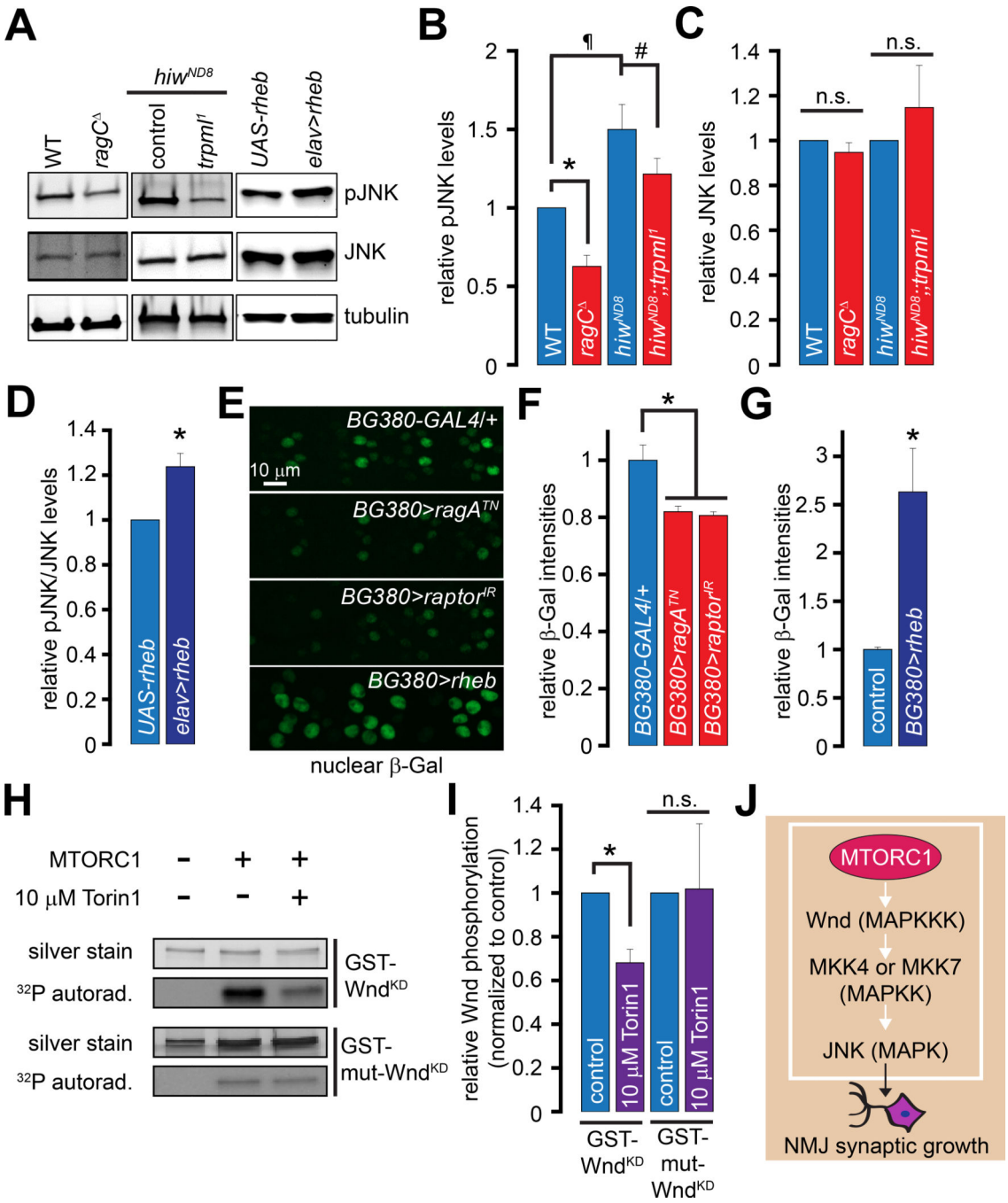

Figure 5. Lysosomal function and Rag/MTORC1 promote Wnd/JNK phosphorylation and *puckered* expression

(A) Western blots performed with larval brain extracts of the indicated genotypes probed with α-pJNK, α-JNK, and α-tubulin primary antibodies.

(B) Bar graph showing the pJNK band intensities normalized to the tubulin band intensities in the indicated genotypes.

(C) Bar graph showing the JNK band intensities normalized to the tubulin band intensities in the indicated genotypes.

Values shown in (B–C) are relative to the WT controls.

(D) Bar graph showing the pJNK/JNK band intensities in the indicated genotypes. The values shown are normalized to the *UAS-rheb* controls.

(E) Representative images showing nuclear β-Gal staining in MN cell bodies in animals of the indicated genotypes. All animals shown in (E) carried the *puc-LacZ* transgene and *UAS-Dicer2*. *UAS-Dicer2* alone did not affect *puc-LacZ* expression (data not shown). The scale bar shown in the top panel applies to all panels. The *BG380>rheb* nuclei are larger consistent with the well-known effects of Rheb to increase cells size in *Drosophila* (Stocker et al., 2003), and the data shown are the average β-Gal intensities over the entire nucleus to control for changes in nuclear size.

(F–G) Bar graph showing relative nuclear β-Gal intensities in the indicated genotypes. The control in (G) is *BG380-GAL4*/+.

(H) *In vitro* kinase assay using purified MTORC1 on recombinant GST-Wnd^{KD} and GST-mut-Wnd^{KD}. Upper panels, silver stain showing total GST-Wnd^{KD} or GST-mut-Wnd^{KD} levels in each sample; Lower panels, ^{32}P autoradiograms showing extent of GST-Wnd^{KD} or GST-mut-Wnd^{KD} phosphorylation in the presence of purified MTORC1 with or without 10 mM Torin1 as indicated.

(I) Bar graph showing quantification of GST-Wnd^{KD} and GST-mut-Wnd^{KD} phosphorylation in the absence (control) or presence of 10 μM Torin1 as indicated. Data shown are normalized to controls.

(J) MTORC1 phosphorylates Wnd resulting in JNK activation and NMJ synaptic growth. MKK4 and MKK7 are MAPKK upstream of JNK (Geuking et al., 2009).

"*", "#", and "¶" represent statistical significance. Abbreviations: n.s., not significant.

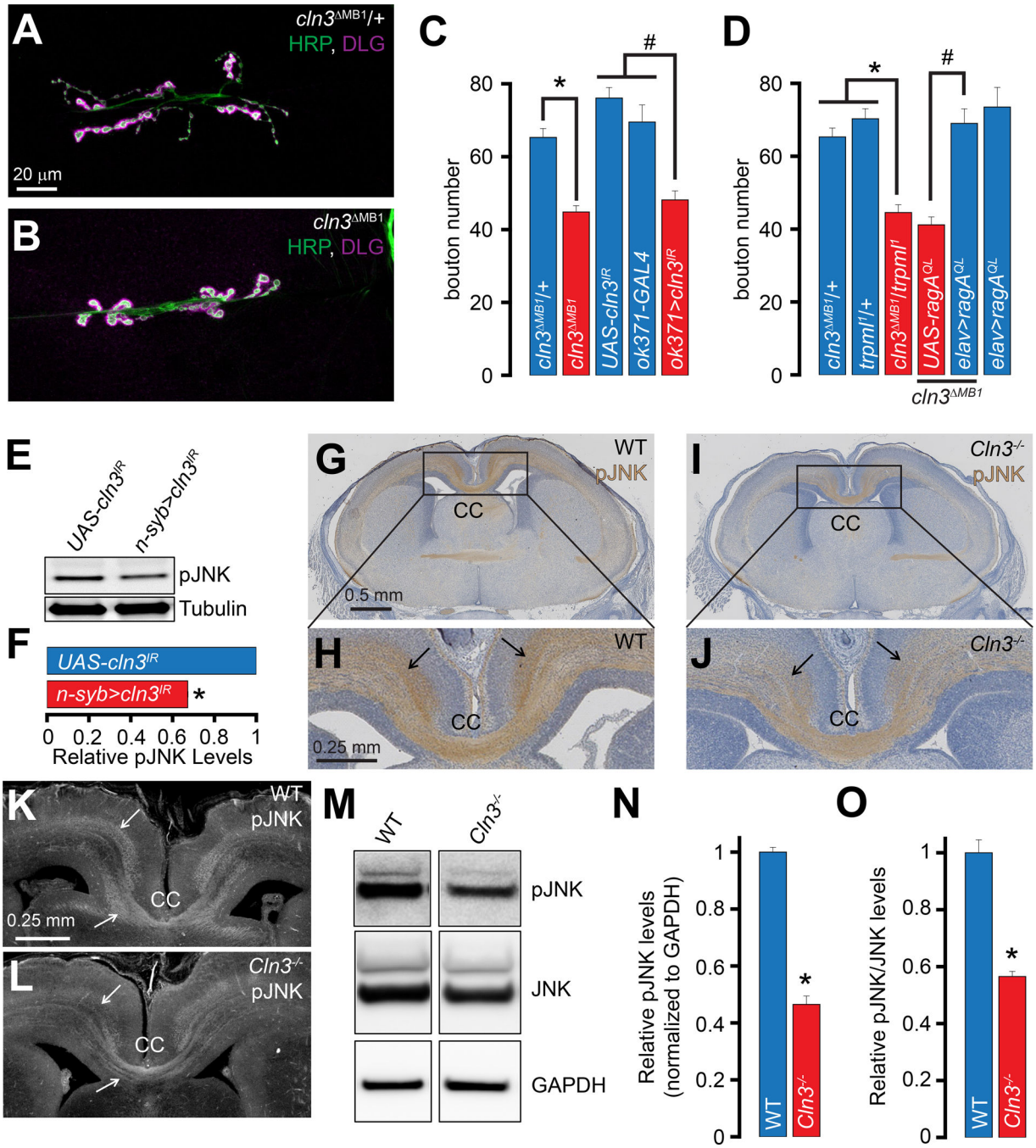

Figure 6. *Drosophila* and mouse models of Batten disease also show diminished neuronal JNK signaling

(A–B) Confocal images of larval NMJs from animals of the indicated genotypes stained with antibodies against HRP (green) and DLG (magenta). Scale bar shown in (A) also applies to (B).

(C–D) Bar graphs showing the average bouton numbers in animals of the indicated genotypes.

(E) Western blots performed with larval brain extracts of the indicated genotypes probed with α-pJNK and α-tubulin primary antibodies.

(F) Bar graph showing the pJNK band intensities normalized to the tubulin band intensities in the indicated genotypes. The values shown are relative to the appropriate *UAS* controls.
(G and I) Coronal sections of E19.5 mouse brains of the indicated genotypes showing α-pJNK staining by immunohistochemistry. Scale bar shown in (G) also applies to (I).
(H and J) Higher magnification of the *boxed* regions from (G) and (I) respectively. Scale bar shown in (H) also applies to (J).
(K–L) Coronal sections of E19.5 mouse brains of the indicated genotypes showing α-pJNK staining by immunofluorescence. Scale bar shown in (K) also applies to (L). *Arrows* in (H, J, and K-L) point to α-pJNK staining in axonal tracts. (M) Western blots performed with cerebral cortex lysates from animals of the indicated genotypes probed with α-pJNK, α-JNK, and α-GAPDH primary antibodies. (N–O) Bar graph showing the relative pJNK band intensities normalized to the GAPDH band intensities in the indicated genotypes (N) and the relative pJNK/JNK band intensities in the indicated genotypes (O). The values shown are relative to the appropriate controls.
"*" represents statistical significance. Abbreviations: n.s., not significant; CC, corpus callosum.

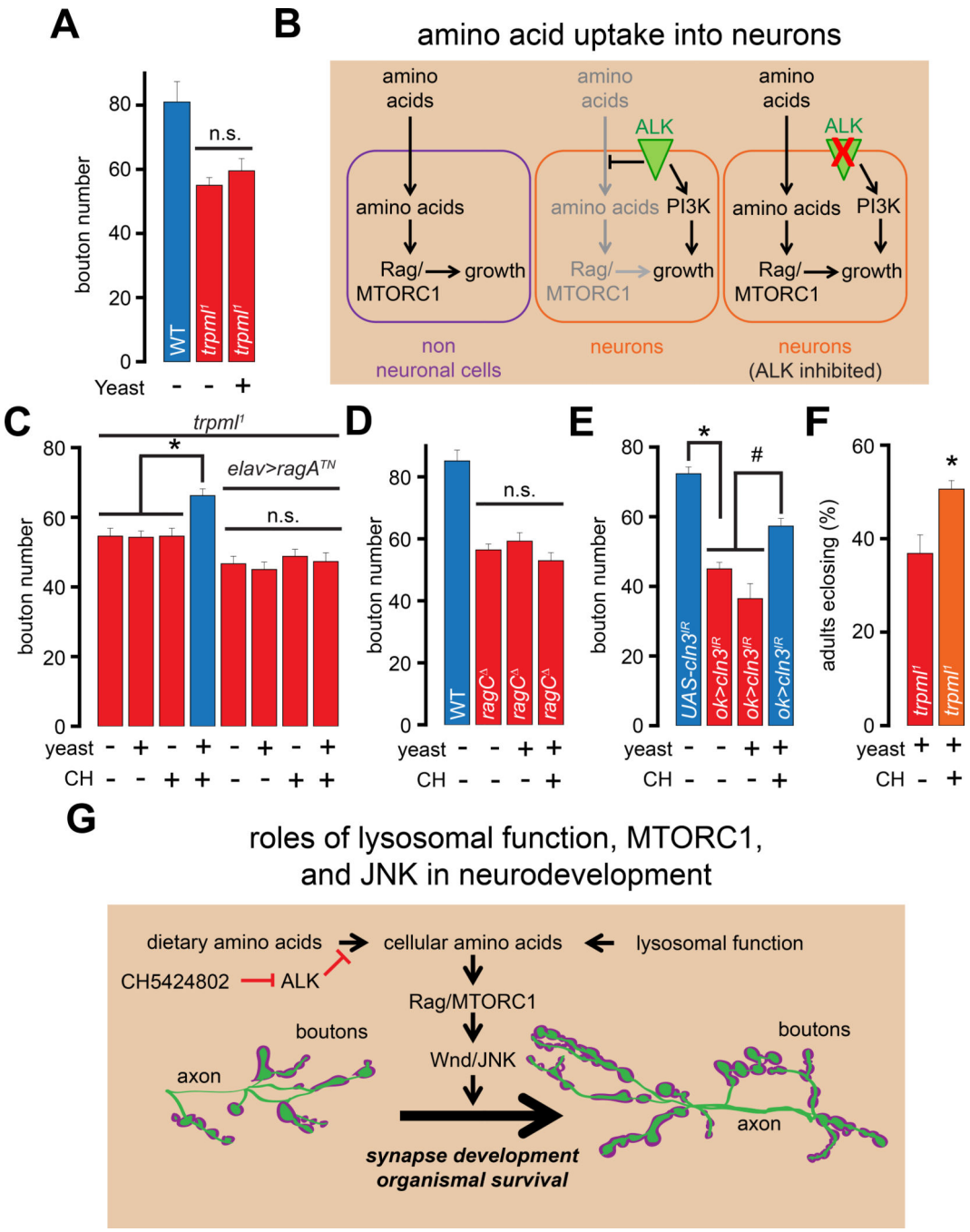

Figure 7. Simultaneous administration of ALK inhibitor and high-protein diet enhances synaptic growth and adult viability following lysosomal dysfunction

(A) Bar graph showing the average bouton numbers in animals of the indicated genotypes reared on instant food with the indicated additions.

(B) Mechanism of ALK-dependent block of amino acid uptake in neuronal cells. (C–E) Bars graph showing the average bouton numbers in animals of the indicated genotypes reared on instant food with the indicated additions.

(F) Bar graph showing the percentage of the *trpml*^{1} adults that eclose from their pupal cases when reared on instant food with the indicated additions. The "+" and "−" in (C–F) represent presence or absence of CH5424802 or yeast. Although rearing larvae on instant food resulted in an overall increase in the number of boutons in all the genotypes, the *trpml*^{1}, *ragC*$^{\Delta}$, and *ok>cln3*^{IR} larvae showed a relative decrease in NMJ boutons, and all comparisons were made between animals reared under identical conditions.

(G) Roles of lysosomal function, MTORC1 activity, Wnd/JNK signaling in neurodevelopment.

"*" and "#" represent statistical significance. Abbreviations: n.s., not significant; CH, CH5424802.